Journal of Solid State Chemistry 183 (2010) 1290–1296

Contents lists available at ScienceDirect

Journal of Solid State Chemistry

journal homepage: www.elsevier.com/locate/jssc

Ab-initio calculation of structural, electronic, and optical characterizations of the intermetallic trialuminides $ScAl_3$ compound

Ali Hussain Reshak [a], Z. Charifi [b,*], H. Baaziz [b]

[a] Institute of Physical Biology-South Bohemia University – Nove Hrady 37333, Czech Republic
[b] Physics Department, Faculty of Science and Engineering, University of M'sila, 28000 M'sila, Algeria

ARTICLE INFO

Article history:
Received 10 December 2009
Received in revised form
15 March 2010
Accepted 21 March 2010
Available online 27 March 2010

Keywords:
FP-LAPW
Optical properties
GGA
EV-GGA

ABSTRACT

We present first-principles study of the electronic and the optical properties for the intermetallic trialuminides $ScAl_3$ compound using the full-potential linear augmented plane wave method within density-functional theory. We have employed the generalized gradient approximation (GGA), which is based on exchange-correlation energy optimization to calculate the total energy. Also we have used the Engel–Vosko GGA formalism, which optimizes the corresponding potential for calculating the electronic band structure and optical properties. The electronic specific heat coefficient (γ), which is a function of density of states, can be calculated from the density of states at Fermi energy $N(E_F)$. The $N(E_F)$ of the phase $L1_2$ is found to be lower than that of $D0_{22}$ structure which confirms the stability of $L1_2$ structure. We found that the dispersion of the band structure of $D0_{22}$ is denser than $L1_2$ phase. The linear optical properties were calculated. The evaluations are based on calculations of the energy band structure.

1. Introduction

The intermetallic trialuminides XAl_3 (X=Zr, Yb and Lu) compounds show a variety of interesting physical properties ranging from magnetism [1–3], de Haas-van Alphen [4,5], thermal [6], transport [7] and electronic properties [8–11]. Among these compounds $ScAl_3$ plays very important role in providing super-plastic ductilities to Al based alloys [12–16]. Superplasticity refers to the ability of a material to pull out to a high tensile elongation without the development of necking within the gauge length [17]. In general, superplasticity is observed in materials having very fine grain sizes, typically less than 10 um, when testing at elevated temperatures where diffusion is reasonably rapid [17,18]. $ScAl_3$, an aluminum rich compound, has received growing attention as high-specific-strength material [19]. Sc is known to give rise to the highest increase in strength, per atomic percent, of any alloying addition in aluminum [20] and it is only slightly denser than aluminum itself [19]. The structural stability and electronic structure of $ScAl_3$ were studied using an all-electron, total energy, and local density approach as implemented in the semirelativistic linear muffin-tin orbital (LMTO) method. The calculated results show that $ScAl_3$ in the $L1_2$ phase is energetically favored compared with the $D0_{22}$ phase by about 0.42 eV per formula unit [8]. And it is found that $ScAl_3$ appears ideal for study as a dispersed phase in aluminum alloys [8]. In addition the optical conductivity of single crystal of $ScAl_3$ was measured by spectroscopic ellipsometry in the range of 1.5–5.5 eV [1]. The conductivity spectra of $ScAl_3$ show peaks between 1.5 and 4.2 eV. To understand the origin of these peaks in the measured optical conducting spectra of $ScAl_3$, Lee et al. [1] employed the FP-LAPW method based on local density approximation (LDA) to calculate density of states and optical conductivity.

Measuring and calculating the optical properties have long been a powerful tool in studying the electronic structure of solids. Today, knowledge of the refractive indices and absorption coefficients of solids is especially important in the design and analysis of new devices. The dielectric function $\varepsilon(\omega)=\varepsilon_1(\omega)+i\varepsilon_2(\omega)$ fully describes the optical properties of any homogeneous medium at all photon energies.

To our knowledge no comprehensive work neither experimental data nor theoretical calculation on the fundamental optical functions of $ScAl_3$ has appeared in the literature. In this paper, we report the calculation of electronic band structure, density of states and for the first time the optical properties such as the dielectric function, reflectivity spectra, refractive index and the loss function. To accomplish that we used the full potential linear augmented plane wave (FP-LAPW) method, which has proven to be one of the most accurate methods [21,22] for the computation of the electronic structure of solids within a framework of density functional theory (DFT). A detailed depiction of the electronic and spectral features of the optical

* Corresponding author. Fax: +213 35 551836.
E-mail addresses: maalidph@yahoo.co.uk (A. Hussain Reshak), charifi_z@yahoo.fr (Z. Charifi).

0022-4596/$ - see front matter © 2010 Elsevier Inc. All rights reserved.
doi:10.1016/j.jssc.2010.03.029

properties of $ScAl_3$ using full potential method is very essential and would bring us important insights in understanding the origin of the electronic band structure and densities of states.

In Section 2 we present the theoretical aspects of the calculation methods. The calculated band structure and density of states are given in the Section 3.1. Section 3.2 is devoted to the optical properties.

2. Theoretical calculation

The intermetallic trialuminides $ScAl_3$ belongs to a $I4/mmm$ for $D0_{22}$ Phase and $Pm3m$ for $L1_2$ space group, the unit cell parameters are given in Table 1. The structure of $L1_2$ and $D0_{22}$ phases are shown in Fig. 1. It was reported in an early study that $ScAl_3$ had the cubic $L1_2$ phase at room temperature [23,24,8]. We use a full-potential linear augmented plane wave method within density-functional theory (DFT) [25], as implemented in the package WIEN2k code [26]. For the exchange and correlation potential we used the generalized gradient approximation (GGA) in the form proposed by Perdew et al. [27] which is based on exchange-correlation energy optimization to calculate the total energy for structural properties. In addition the Engel–Vosko generalized gradient approximation (EV-GGA) [28], which optimizes the corresponding potential, is used for band structure and optical properties calculations. It is well known that the DFT self-consistent band structure calculations using either LDA or GGA functional, usually underestimate the energy gap of semiconductors [29]. This is mainly due to the fact that they have simple forms that are not sufficiently flexible to accurately reproduce both exchange-correlation energy and its charge derivative. Engel and Vosko considered this shortcoming and constructed a new functional form of GGA, which is able to better reproduce the exchange potential at the expense of less agreement in the exchange energy. This approach called EV-GGA, yields better band splitting and some other properties which mainly depend on the accuracy of exchange correlation potential. We take the full relativistic effects for core states and use the scalar relativistic approximation for the valence states. The R_{MT} are assumed to be 2.0 atomic units (a.u.) for Sc and 1.9 a.u. for Al. We used the parameters $K\max=9/R_{MT}$ and $l_{max}=10$. The self-consistency was achieved by using 84 k-points for $L1_2$ and 99 k-points for $D0_{22}$ in the irreducible Brillouin zone (IBZ). The density of states and the optical properties are calculated using 286 and 726 k-points for $L1_2$ and $D0_{22}$, respectively. The self-consistent interactions were performed until the convergence in the energy reaches about 10^{-4} Ry. Five to seven values of c/a are typically used for a fixed volume and a polynomial is then fitted to the calculated energies to determine the best c/a ratio. The final outcome of this process is a set of values of the equilibrium cell energy versus the cell volume: $E(V)=\min_{c/a} E(V,c/a)$. We have calculated the total energy at several volumes around the equilibrium for the investigated compound as illustrated in Fig. 2. It is clearly seen that the $L1_2$ phase is energetically favored compared to the $D0_{22}$ phase in the entire region shown. This is in good agreement with the results obtained by Xu and Freeman [8].

3. Results and discussion

3.1. Band structure and density of states

The electronic band structures along the symmetry lines of the Brillouin zone using EV-GGA approximation are shown in Fig. 3. The total density of states along with the Sc-s/p/d and Al-s/p partial densities of states were calculated and illustrated in Fig. 4. We note that moving from $L1_2$ to $D0_{22}$ all the structures in the

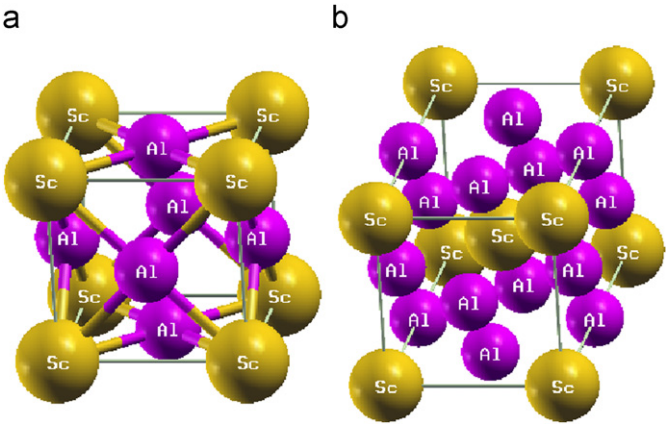

Fig. 1. Crystal structure of $L1_2$ (a) and $D0_{22}$ (b) phases of $ScAl_3$ compound.

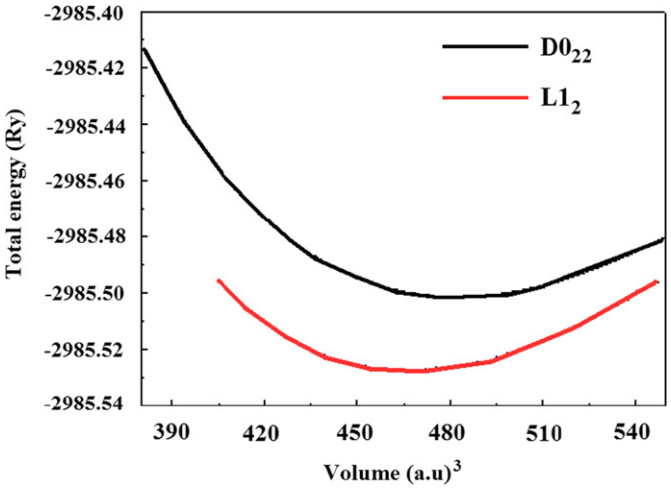

Fig. 2. Variation of total energies as a function of volume for $L1_2$ and $D0_{22}$ phases of $ScAl_3$ compound calculated using the GGA approximation.

Table 1
Calculated lattice parameters, bulk modulus, its derivative and DOS at E_F, in comparison with the available previous calculations and the experimental data for $ScAl_3$ compounds in two phases.

$ScAl_3$	a (Å)			c/a		B (GPa)	B'	$N(E_F)$ (states/eV)
	Structure	Calc.	Exp.	Calc.	Exp.			
	$L1_2$	4.104*, 4.055[8]	4.10 [23]			86.48*, 93 [8]	4.39*	1.28, 1.165 [8]
	$D0_{22}$	4.29*, 3.966[8]		2.22*, 2.21 [8]		81.285*, 90 [8]	3.912*	2.37, 1.805 [8]

* This work.

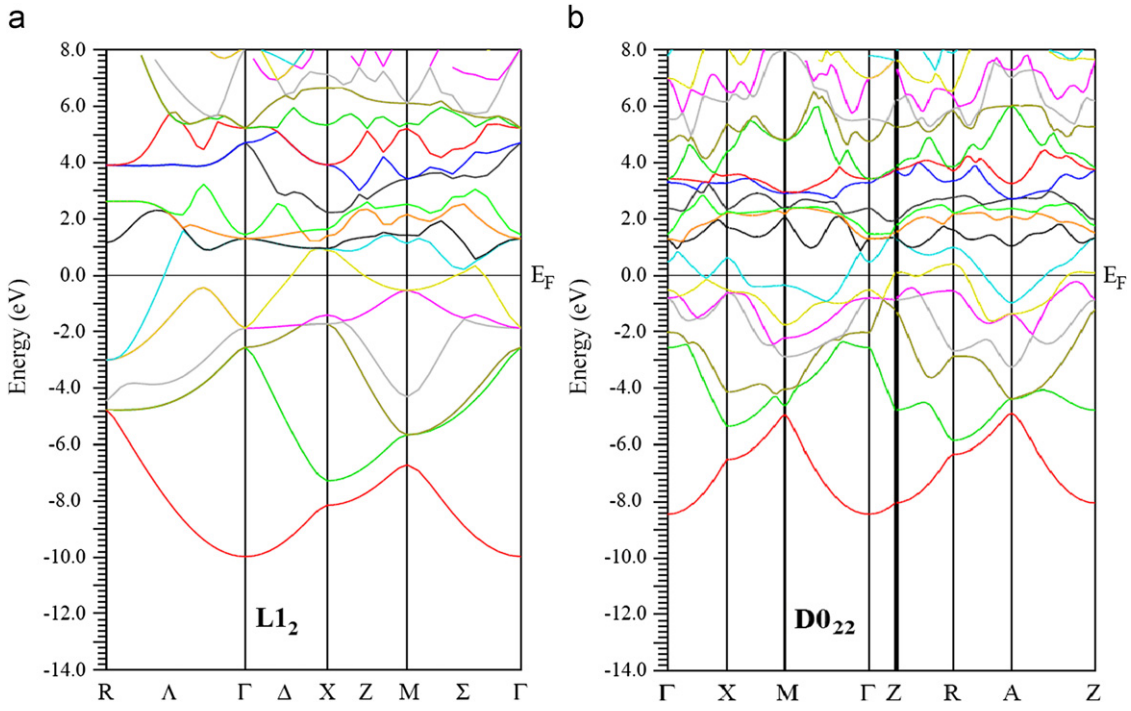

Fig. 3. Calculated band structures using EV-GGA for the two phases (a) $L1_2$ and (b) $D0_{22}$ of $ScAl_3$ compound.

DOS and the electronic band structure shift towards higher energies resulting in pushing more bands towards E_F and more bands cut E_F indicating that the compound becomes more metallic with density of states at Fermi energy (E_F) of about 17.37 and 32.18 (states/Ry-cell) for $L1_2$ and $D0_{22}$, respectively. We note that the cubic $ScAl_3$ phase has a low $N(E_F)$ value which confirms the stability of this phase [30,31]. It is clear that the dispersion of the band structure of $D0_{22}$ is denser than that of $L1_2$. The DOS at Fermi energy (E_F) is determined by the overlap between the valence and conduction bands. This overlap is strong enough indicating metallic origin with different values of DOS at E_F, $N(E_F)$. The electronic specific heat coefficient (γ), which is a function of density of states, can be calculated using the expression, $\gamma = \frac{1}{3}\pi^2 N(E_F)k_B^2$, here $N(E_F)$, is the density of states at Fermi energy, and k_B is the Boltzmann constant. The calculated density of state at Fermi energy $N(E_F)$, enables us to calculate the bare electronic specific heat coefficient, the obtained value is about 3.0132 and 5.5824 (mJ/mol.K^2) for $L1_2$ and $D0_{22}$, respectively. It is clear that when we move from $L1_2$ phase to the $D0_{22}$ phase the overlapping around E_F is increased. From the PDOS one can see that all the Sc-d states concentrated at the conduction bands with very small contribution around Fermi energy. Moving from $L1_2$ to $D0_{22}$ we notice that: (1) more Sc-d bands overlapping around Fermi energy with increasing the magnitude of Sc-d in the conduction band. (2) Sc-s hybridizes strongly with Sc-p, whereas the hybridization reduces between Al-p and Al-s around 2.0 eV in the $D0_{22}$ phase in comparison with $L1_2$ phase, which is attributed to the increasing of the Al-p magnitude and reducing the magnitude of Al-s when we move from $L1_2$ to $D0_{22}$ phase.

3.2. Optical properties

The I4/mmm space group of $ScAl_3$ with two formula units per unit cell, has two dominant components of the dielectric tensor. These frequency-dependent dielectric functions are $\varepsilon_2^{\parallel}(\omega)$ and $\varepsilon_2^{\perp}(\omega)$ corresponding to the electric field direction parallel and perpendicular to the crystallographic c axis. We have performed calculations of the imaginary part of the interband frequency dependent dielectric function using the expressions in Ref. [32].

$$\varepsilon_2^{\parallel}(\omega) = \frac{12}{m\omega^2}\int_{BZ}\sum_{n,n'}\frac{|P^Z_{nn'}(k)|^2 dS_k}{\nabla\omega_{nn'}(k)}$$

$$\varepsilon_2^{\perp}(\omega) = \frac{6}{m\omega^2}\int_{BZ}\sum_{n,n'}\frac{[|P^X_{nn'}(k)|^2 + |P^Y_{nn'}(k)|^2]dS_k}{\nabla\omega_{nn'}(k)}$$

The above expressions are written in atomic units with $e^2 = 1/m = 2$ and $\hbar = 1$, where ω is the photon energy. $P^X_{nn'}(k)$ and $P^Z_{nn'}(k)$ are the X and Z component of the dipolar matrix elements between initial $|nk\rangle$ and final $|n'k\rangle$ states with their eigenvalues $E_{n(k)}$ and $E_{n'}(k)$, respectively.

$\omega_{n'}(k)$ is the energy difference $\omega_{nn'}(k) = E_n(k) - E_{n'}(k)$ and S_k is a constant energy surface $S_k = \{k, \omega_{nn'}(k) = \omega\}$. The integral is over the first Brillouin zone.

Whereas the space group Pm3m has only one component of the dielectric tensor. For this space group we have calculated the imaginary part of the frequency-dependent dielectric functions using the expression in Ref. [33].

$$\varepsilon_2(\omega) = \frac{8}{3\pi\omega^2}\sum_{nn'}\int_{BZ}|\mathbf{P}_{nn'}(k)|^2\frac{dS_k}{\nabla\omega_{nn'}(k)}$$

where $\mathbf{P}_{nn'}(k)$ is the dipolar matrix elements between initial $|nk\rangle$ and final $|n'k\rangle$ states with their eigenvalues $E_{n(k)}$ and $E'_n(k)$, respectively.

The calculation of these frequency dependent dielectric functions requires the precise values of energy eigenvalues and electron wavefunctions. These are natural outputs of a band structure calculation. Generally there are two contributions to frequency-dependent dielectric functions, namely intra-band and inter-band transitions. The contribution due to intra-band transitions is crucial only for metals. The inter-band transitions of these frequency-dependent dielectric functions can be split into direct and indirect transitions. We neglect the indirect inter-band transitions involving scattering of phonons assuming that they give a small contribution to

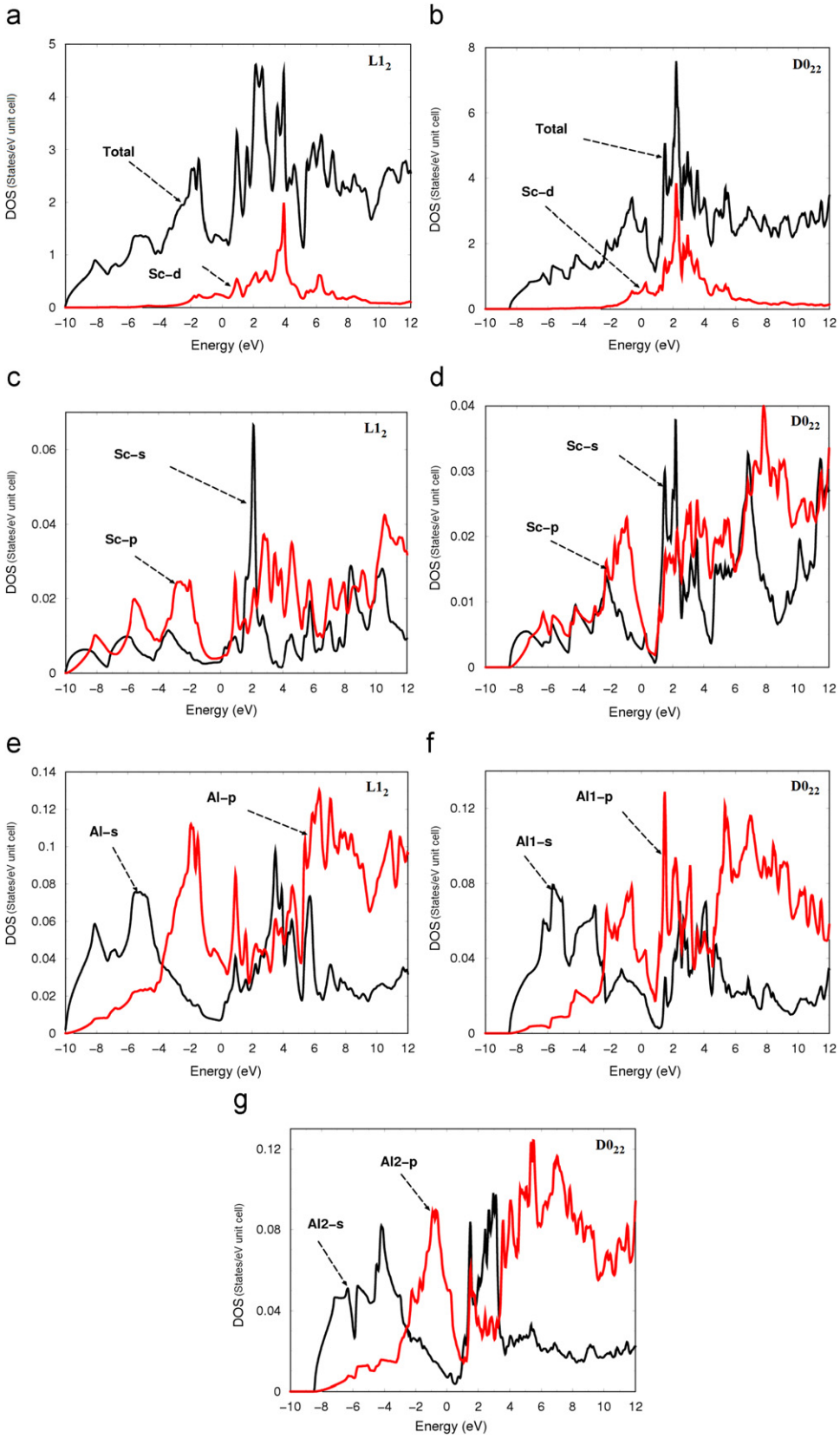

Fig. 4. The total and partial density of states (states/eV unit cell) $L1_2$ and $D0_{22}$ phases.

the frequency-dependent dielectric functions. To calculate the direct inter-band contributions to the imaginary part of the frequency-dependent dielectric function, it is necessary to perform summation over the BZ structure for all possible transitions from the occupied to the unoccupied states taking the appropriate transition dipole matrix elements into account.

Fig. 5a and b, depicts the variation of the imaginary part of the frequency dependent dielectric function. The spectral broadening

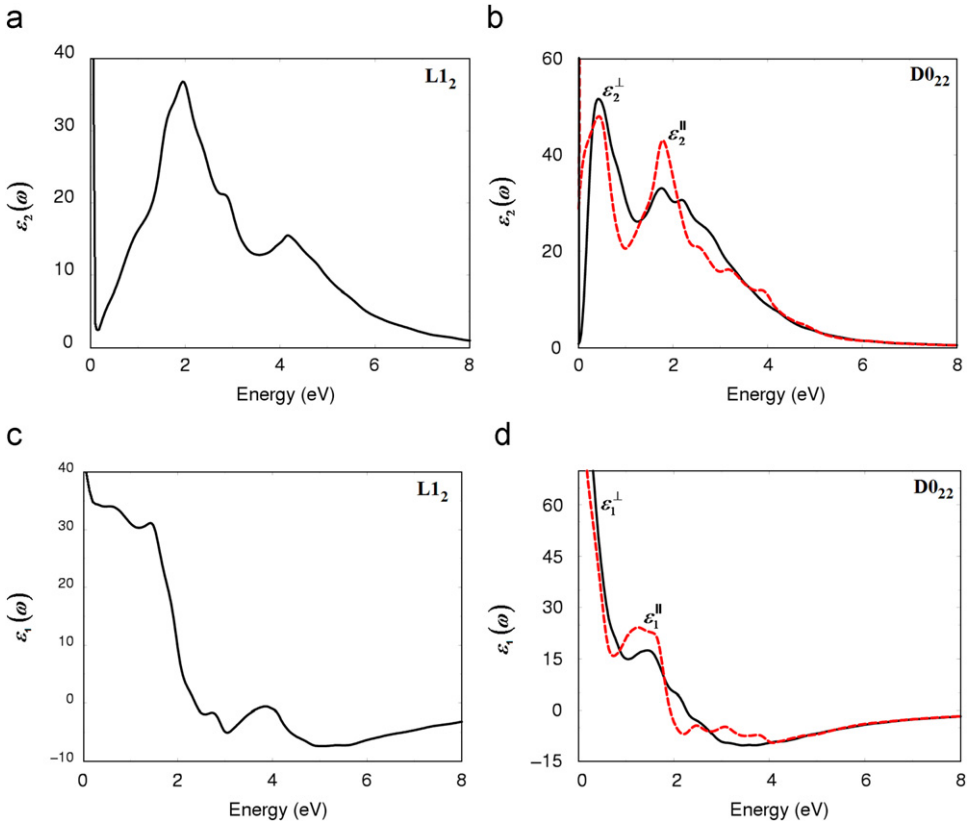

Fig. 5. Calculated imaginary (a) and (b) and real parts (c) and (d) of the frequency dependent dielectric function for $ScAl_3$ compound in $L1_2$ and $D0_{22}$ phases using EV-GGA.

is taken to be 0.1 eV. We have included the Drude term, its effect is significant for energies less than 1 eV. The sharp rise at low energies is due to the Drude term. Following $\varepsilon_2(\omega)$ spectra one can conclude that the $L1_2$ phase shows one principal peak situated around 2.0 eV, whereas the $D0_{22}$ phase shows two principal peaks situated around 0.5 and 2.0 eV for $\varepsilon_2^{\perp}(\omega)$ and $\varepsilon_2^{\parallel}(\omega)$, respectively. We should emphasize that there is a considerable anisotropy between these two components $\varepsilon_2^{\parallel}(\omega)$ and $\varepsilon_2^{\perp}(\omega)$ of $D0_{22}$. The peaks in the optical response are caused by the allowed electric–dipole transitions between the valence and conduction bands. To identify these structures we should consider the magnitude of the optical dipole matrix elements. The observed structures would correspond to those transitions which have larger optical matrix dipole transition elements. It would be worthwhile to attempt to identify the inter-band transitions that are responsible for the spectral features in $\varepsilon_2(\omega)$ and $\varepsilon_2^{\parallel}(\omega)$ and $\varepsilon_2^{\perp}(\omega)$ using our calculated band structure and density of states. The optical transitions occur between the occupied states Sc-s/p/d and Al-s/p and the unoccupied states Sc-s/p/d and Al-s/p. Also we have calculated the real parts of the dielectric functions. The real parts of the frequency dependent dielectric function $\varepsilon_2^{\parallel}(\omega)$ and $\varepsilon_1^{\perp}(\omega)$can be derived from the imaginary part using the Kramers–Kronig relations [34] (see Fig. 5 c and d).

For more details about the spectral features of the optical properties of the investigated crystal we have calculated the reflectivity spectra $R(\omega)$, refractive indices $n(\omega)$ and loss function $L(\omega)$. Fig. 6a and b, shows the calculated reflectivity spectra. We notice that a reflectivity maximum between 5.0 to 11.0 eV for $D0_{22}$ and 8.0 to 11.0 for $L1_2$ arises from inter-band transitions. We noticed that there is an abrupt reduction in the reflectivity spectrum at 12.66 and 13.09 eV for $R^{\parallel}(w)$ and $R^{\perp}(\omega)$ of $D0_{22}$ phase, respectively, and at 13.09 eV of $L1_2$ phase which confirms the occurrence of a collective plasma resonance. The depth of the plasma minimum is determined by the imaginary part of the dielectric function at the plasma resonance and is representative of the degree of overlap between the inter-band absorption regions. The calculated refractive indices $n(\omega)$ are shown in Fig. 6c and d. We note that at low energy range both of $L1_2$ and $D0_{22}$ shows high refractive indices then goes to lower values at the high energies. There is a considerable anisotropy between the two components of $D0_{22}$ phase. Electron energy loss spectroscopy (EELS) is a valuable tool for investigating various aspects of materials [35]. It has the advantage of covering the complete energy range including non-scattered and elastically scattered electrons (zero loss). At intermediate energies (typically 1–50 eV), the energy losses are primarily due to a complicated mixture of single electron excitations and collective excitations (plasmons). The positions of the single electron excitation peaks are related to the joint density of states between the conduction and valence bands, whereas the energy required for the excitation of bulk plasmons depends mainly on the electron density in the solid. At higher energies, typically a few hundred eV, edges can be seen in the spectrum, indicating the onset of excitations from the various inner atomic shells to the conduction band. In this case, the fast electrons excite the inner shell electrons (core loss) or induce core level excitation of near edge structure (ELNES) and X-ray absorption near edge structure (XANES). The edges are characteristic of particular elements and their energy and height can be used for elemental analysis. Plasmon losses correspond to a collective oscillation of the valence electrons and their energy is related to the density of valence electrons. In the case of inter-band transitions, which consist mostly of plasmon excitations, the scattering probability for volume losses is directly connected to the energy loss function. In Fig. 6e and f, the energy loss function is plotted in basal-plane and in direction of c-axis. There are other features in this spectrum, in addition to the plasmon peak,

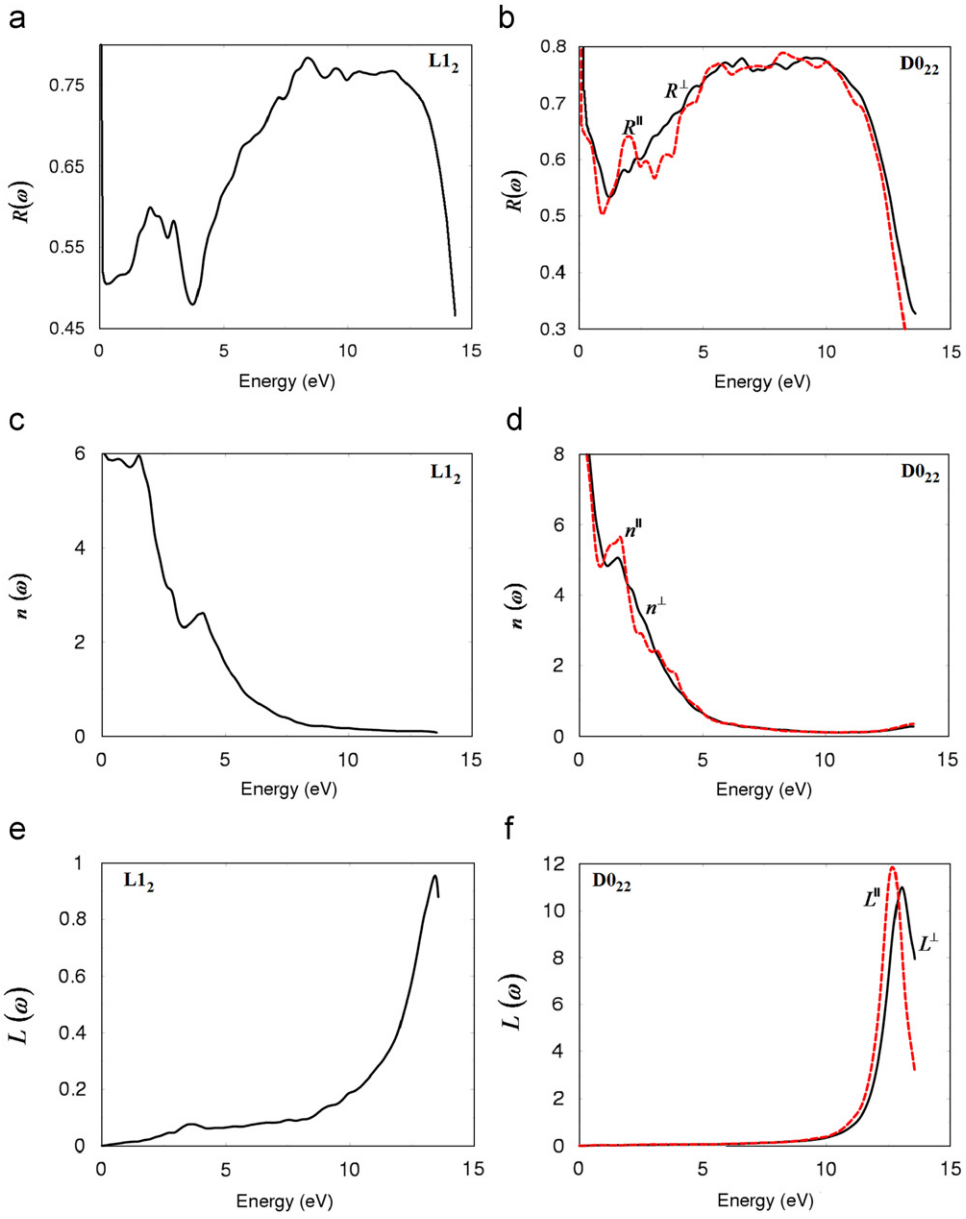

Fig. 6. Calculated reflectivity (a) and (b), refractive indices (c) and (d) and electron energy loss (e) and (f) for $L1_2$ and $D0_{22}$ phases of $ScAl_3$ compound using EV-GGA.

associated with interband transitions. The plasmon peak is usually the most intense feature in the spectrum and this is at energy where $\varepsilon_1(\omega)$ goes to zero. For our compound, the energy of the maximum peak of $(-\varepsilon_1(\omega))^{-1}$ at $\sim$12.66 eV for $L^{\parallel}(\omega)$ and 13.09 eV for $L^{\perp}(\omega)$ of $D0_{22}$ and around 13.06 eV for $L1_2$ which are assigned to the energy of volume plasmon ω_p. As there are no experimental or theoretical results for the spectral features of the optical properties available for these compounds, we hope that our work will stimulate more works.

4. Summary and conclusions

We have performed first principles calculations of the electronic properties such as the electronic band structure, density of states, linear optical properties within a framework of FP-LAPW method. The evaluations are based on calculations of the energy band structure. The imaginary and real parts of the frequency dependent dielectric function, reflectivity and loss function were calculated and analyzed based on our calculated band structure and density of states. The linear optical properties of $D0_{22}$ show a considerable anisotropy. The density of states at Fermi energy (E_F) increases when we move from $L1_2$ to $D0_{22}$ and the dispersion of the band structure of $D0_{22}$ is denser than that of $L1_2$.

The DOS at Fermi energy (E_F) and the electronic specific heat coefficient (γ) were determined. It is clear that the overlapping around E_F is increased when we move from $L1_2$ phase to the $D0_{22}$ phase. All the Sc-d concentrated at the conduction bands with very small contribution around Fermi energy. Moving from $L1_2$ to $D0_{22}$ we notice that: (1) more Sc-d bands overlapping around Fermi energy with increasing the magnitude of Sc-d in the conduction band. (2) Sc-s hybridizes strongly with Sc-p, whereas the hybridization reduces between Al-p and Al-s around 2.0 eV that is attributed to the increasing of the Al-p magnitude and reducing the magnitude of Al-s.

The optical properties of the investigated crystal $\varepsilon_2(\omega)$, $\varepsilon_2^{\parallel}(\omega)$, $\varepsilon_2^{\perp}(\omega)$, $R(\omega)$, $n(\omega)$ and loss function $L(\omega)$ were calculated and analyzed using our calculated density of states and the electronic

band structure. We should emphasize that in the $L1_2$ phase $\varepsilon_2(\omega)$ shows one principal peak situated around 2.0 eV, whereas in the $D0_{22}$ phase it shows two principal peaks situated around 0.5 and 2.0 eV for $\varepsilon_2^{\perp}(\omega)$ and $\varepsilon_2^{\parallel}(\omega)$, respectively. In addition it is noticed that there is an abrupt reduction in the reflectivity spectrum at 12.66 and 13.09 eV for $R^{\parallel}(\omega)$ and $R^{\perp}(\omega)$ of $D0_{22}$ phase, respectively, and at 13.09 eV of $L1_2$ phase which confirms the occurrence of a collective plasma resonance. The calculated refractive indices $n(\omega)$ reveal that at low energy range both of $L1_2$ and $D0_{22}$ show high refractive indices then go to lower values at the high energies.

Acknowledgments

This work was supported from the institutional research concept of the Institute of Physical Biology, UFB (no. MSM6007665808).

References

[1] S.J. Lee, J.M. Park, P.C. Canfield, D.W. Lynch, Phys. Rev. B 67 (2003) 075104.
[2] A. Hiess, J.X. Boucherle, F. Givord, J. Schweizer, E. Lelievre- Berna, F. Tasset, B. Gillon, P.C. Canfield, J. Phys.: Condens. Matter 12 (2000) 829.
[3] C.M. Varma, Y. Yafet, Phys. Rev. B 13 (1976) 2950.
[4] T. Ebihara, S. Uji, C. Terakura, T. Terashima, E. Yamamoto, Y. Haga, Y. Inada, Y. Onuki, Physica B 281–282 (2000) 754.
[5] I. Sakamoto, G.F. Chen, S. Ohara, H. Harima, S. Maruno, J. Alloys Compd. 323–324 (2001) 623.
[6] D.M. Rowe, G. Min, V. Kuznetsov, S.G.K. Williams, Adv. Sci. Technol. (Faenza, Italy) 24 (1999) 793.
[7] S. Ohara, G.F. Chen, I. Sakamoto, J. Alloys Compd. 323–324 (2001) 632.
[8] J.-H. Xu, A.J. Freeman, Phys. Rev. B 41 (1990) 12553.
[9] K. Takegahara, Physica B 186–188 (1993) 850.
[10] S.-J. Oh, S. Suga, A. Kakizaki, M. Taniguchi, T. Ishii, J.-S. Kang, J.W. Allen, O. Gunnarsson, N.E. Christensen, A. Fujimori, T. Suzuki, T. Kasuya, T. Miyahara, H. Kato, K. Schonhammer, M.S. Torikachvili, M.B. Maple, Phys. Rev. B 37 (1988) 2861.
[11] G. Bester, M. Fähnle, J. Phys.: Condens. Matter 13 (2001) 11551.
[12] H.B. Hyde, A.F. Norman, R.B. Prangnell, Acta Mater. 49 (2001) 1327.
[13] S. Lee, A. Utsunomiya, H. Akamatsu, K. Neishi, M. Furukawa, Z. Horita, T.G. Langdon, Acta Mater. 50 (2002) 553.
[14] G.M. Novotny, A.J. Ardell, Mater. Sci. Eng. A Struct. Mater. Prop. Microstruct. Process 318 (2001) 144.
[15] Q.L. Pan, Z.M. Yin, J.X. Zou, X.M. Chen, C.F. Zhang, Acta Metall. Sin. 37 (2001) 749.
[16] M. Oku, T. Shishido, Q. Sun, K. Nakajima, Y. Kawazoe, K. Wagatsuma, J. Alloys Compd. 358 (2003) 264.
[17] S. Lee, A. Utsunomiya, H. Akamatsu, K. Neishi, M. Furukawa, Z. Horita, T.G. Langdon, Acta Materialia 50 (2002) 553–564.
[18] T.G. Langdon, Metall. Trans. 13A (1982) 689.
[19] M. Asta, V. Ozolins, Phys. Rev. B 64 (2001) 094104.
[20] M.E. Drits, L.S. Toropova, R.L. Gushchina, S.G. Fedotov, J. Sov. N. Ferrous Met. Res. 12 (1984) 83.
[21] S. Gao, Comput. Phys. Commun. 153 (2003) 190.
[22] K. Schwarz, J. Solid State Chem. 176 (2003) 319.
[23] V.W. Rechkin, L.K. Lamikhov, T.I. Samsonova, Kristallografiya 9 (1964) 405.
[24] T.B. Massalski (Ed.), Binary Alloy Phase Diagrams, 1, American Society for Metals, Metals Park, Ohio, 1986, p. 822.
[25] P. Hohenberg, W. Kohn, Phys. Rev. B 136 (1964) 864.
[26] P. Blaha, K. Schwarz, G.K.H. Madsen, D. Kvasnicka, J. Luitz, WIEN2K, an Augmented Plane Wave+Local orbitals program for calculating crystal properties, Karlheinz Schwarz, Techn. Universitat, Wien, Austria, 2001, ISBN:3-9501031-1-2.
[27] J.P. Perdew, S. Burke, M. Ernzerhof, Phys. Rev. Lett. 77 (1996) 3865.
[28] E. Engel, S.H. Vosko, Phys. Rev. B 47 (1993) 13164.
[29] P. Dufek, P. Blaha, K. Schwarz, Phys. Rev. B 50 (1994) 7279.
[30] J.-H. Xu, T. Oguchi, A.J. Freeman, Phys. Rev. B 35 (1987) 6940.
[31] J.-H. Xu, A.J. Freeman, Phys. Rev. B 40 (1989) 11927.
[32] S. Hufner, R. Claessen, F. Reinert, T.h. Straub, V.N. Strocov, P. Steiner, J. Electron Spectrosc. Relat. Phenom. 100 (1999) 191;
R. Ahuja, S. Auluck, B. Johansson, M.A. Khan, Phys. Rev. B 50 (1994) 2128.
[33] M.A. Khan, A. Kashyap, A.K. Solanki, T. Nautiyal, S. Auluck, Phys. Rev. B 23 (1993) 16974.
[34] F. Wooten, Optical Properties of Solids, Academic press, New York and London, 1972.
[35] S. Loughin, R.H. French, L.K. De Noyer, W.-Y. Ching, Y.-N. Xu, J. Phys. D: Appl. Phys. 29 (1996) 1740.